

# OPTIMISATION OF JET-DT AND ITER OPERATION BY DEVELOPING AN UNDERSTANDING OF THE ROLE OF LOW-Z IMPURITY ON THE H-MODE PEDESTAL

C. Giroud<sup>1</sup>, N. Aiba<sup>2</sup>, A. Chankin<sup>3</sup>, D. Hatch<sup>4</sup>, M. Kotschenreuther<sup>4</sup>, D. Moulton<sup>1</sup>, J. Parisi<sup>5,1</sup>, F. Parra<sup>5,1</sup>, S. Buller<sup>9</sup>, C. Challis<sup>1</sup>, J. Harrison<sup>1</sup>, J. Hillesheim<sup>1</sup>, L. Horvath<sup>6</sup>, H-T. Kim<sup>1</sup>, D. Frigione<sup>7</sup>, B. Lomanowski<sup>8</sup>, F. Militello<sup>1</sup>, S. Pamela<sup>1</sup>, I. Pusztai<sup>9</sup>, D. Refy<sup>10</sup>, S. Saarelma<sup>1</sup>, C. Stavrou<sup>8</sup>, B. Tal<sup>10</sup>, M. Barnes<sup>5,1</sup>, E. Belonohy<sup>1</sup>, S. Brezinsek<sup>11</sup>, C. Bowman<sup>6</sup>, E. Delabie<sup>12</sup>, A. Field<sup>1</sup>, J. Fontdecaba<sup>13</sup>, A. Huber<sup>11</sup>, A. Meigs<sup>1</sup>, S. Menmuir<sup>1</sup>, J. Simpson<sup>1</sup> and JET Contributors\*.

EUROfusion Consortium, JET, Culham Science Centre, Abingdon, OX14 3DB, UK

<sup>1</sup> Culham Centre for Fusion Energy, Culham Science Centre, Abingdon OX14 3DB, UK

<sup>2</sup> National Institutes for Quantum and Radiological Science and Technology, Rokkasho, Aomori 039-3212, Japan

<sup>3</sup> Max-Planck-Institut für Plasmaphysik, D-85748 Garching, Germany

<sup>4</sup> Institute for Fusion Studies, University of Texas at Austin, Austin, TX 78712, USA

<sup>5</sup> Rudolf Peierls Centre for Theoretical Physics, University of Oxford, Oxford OX1 3NP, UK

<sup>7</sup> University of York, Heslington, York YO10 5DD, UK

<sup>6</sup> Unità Tecnica Fusione - ENEA C. R. Frascati - via E. Fermi 45, 00044 Frascati (Roma), Italy

<sup>8</sup> Aalto University, P.O.Box 14100, FIN-00076 Aalto, Finland

<sup>9</sup> Department of Physics, Chalmers University of Technology, SE-41296, Gothenburg, Sweden

<sup>10</sup> Wigner Research Centre for Physics, P.O.B. 49, H - 1525 Budapest, Hungary

<sup>11</sup> Forschungszentrum Jülich, Institut für Energie-und Klimaforschung - Plasmaphysik, 52425 Jülich, Germany

<sup>12</sup> Oak Ridge National Laboratory, Oak Ridge, TN 37831-6169, Tennessee, USA

<sup>13</sup> Laboratorio Nacional de Fusión, CIEMAT, Madrid, Spain

\* See the author list of X. Litaudon et al 2017 Nucl. Fusion 57 102001

e-mail: [carine.giroud@ukaea.uk](mailto:carine.giroud@ukaea.uk)

## Abstract

Robust predictions for the pedestal height in ITER require an understanding of the role of D-gas and impurity injection, such as N and Ne, on the pedestal temperature and density in JET-ILW both in terms of loss of pedestal pressure and/or temperature (with D-gas and Ne) as well as its improvement (with N or C). On JET-ILW, seeding Ne can result in either a decrease or increase on the pedestal density depending on pedestal collisionality and  $\beta_N$ , but in all cases seeding Ne does not lead to an increase of temperature, unlike with C. Seeding C<sub>2</sub>D<sub>4</sub> counteracts the electron temperature and density degradation of a high D-gas rate injection. The maximum normalised pressure gradient in the pedestal of the low and high- $\beta_N$  plasmas is within 20% of the critical normalised pressure gradient calculated a linear MHD code taking the effect of the ion diamagnetic effect and rotation on the stability. ETG instability is identified to be the dominant energy loss mechanism for the low and high- $\beta_N$  plasmas but can also drive instabilities in the ion scale level.

## 1. INTRODUCTION

Impurity seeding via injection of neon (Ne) or nitrogen (N) will be mandatory in ITER Q=10 reference scenario to reduce inter-ELM power load to the divertor within the engineering limits. The challenge is achieving the scenario requirement of  $H_{98(y,2)}=1$ ,  $\beta_N =1.8$ ,  $\langle n \rangle/n_{GW} =0.85$ ,  $\delta=0.4$ , with a highly radiative divertor. These conditions necessitate a high pedestal temperature which leads the pedestal to play a key role in this challenging integration and obtaining reliable predictions. The predictions for the pedestal temperature and pressure in ITER have been put to a test with the reduction in the pedestal pressure in JET with its metallic ITER-like wall (JET-ILW) with reference to the carbon wall phase of JET (JET-C). In JET-ILW, a reduction in the pedestal temperature is observed in all scenarios regardless of the level of D-gas injection or value of normalised pressure  $\beta_N$  [1] [2] [3]. At low D-gas injection, high W radiation is not always the cause for this reduction.

Unravelling the mechanism that, in the absence of carbon in the plasma composition leads to a decrease in the pedestal temperature is critical in predicting the pedestal pressure in ITER. It is particularly important to learn how to use the extrinsic impurity to optimise the pedestal temperature in highly radiative scenarios. The understanding of these mechanisms would also be beneficial in keeping a pedestal temperature as high as possible in the future JET DT scenarios (with  $H_{98(y,2)}>1$ ,  $\beta_N >1.8$ ,  $\langle n \rangle/n_{GW} \sim 0.6$ ,  $\delta=0.2$ ) where Ne-seeding for power load control is one of the routes envisaged to achieve the requirement of 15MW fusion power for 5s. This paper aims at (1) deepening our understanding of the effect of carbon (C), N and Ne-seeding on the pedestal pressure and temperature, (2) assessing whether the peeling ballooning stability limits the pedestal pressure, and (3)

determining which instabilities are causing heat and particle transport. This will allow us to lay the foundations for ITER predictions.

## 2. DESCRIPTION OF THE EXPERIMENTS

In JET-ILW the limitation on the pedestal temperature is alleviated partially with the injection of N, in the high- $\delta$  baseline (2.5MA/2.7T, P<sub>nbi</sub>=16MW,  $\beta_N=1.2$ ,  $\delta=0.4$ ) where the pre-ELM pedestal pressure is increased via an increasing both the pedestal temperature and density [4]. In contrast, Ne-seeding decreased the pedestal temperature and density in these discharges [5]. The low- $\beta_N$  plasmas at high pedestal collisionality value,  $v_e^* > 1.5$ , were first investigated as a direct comparison between well diagnosed JET-C and JET-ILW plasmas was possible, as well as being the ITER baseline reference scenarios. However, our understanding of the effect of impurity and D-gas need to be also extended to pedestal conditions relevant to JET-DT, i.e. a lower pedestal collisionality ( $v_e^* \sim 0.26$ ) and a target  $\beta_N > 1.8$  at low triangularity ( $\delta=0.2$ ). Experiments have then been carried out in high- $\beta_N$  plasmas (1.4MA/1.9T, P<sub>nbi</sub>~16.5-17.5,  $\beta_N=2.5$ ,  $\delta=0.2$  with  $P_{sep}/P_{LH}>2$ ) at a lower collisionality,  $v_e^* = 0.1-0.6$  and low current to avoid additional operational limitation due to excessive W radiation. A scan in D-gas, C<sub>2</sub>D<sub>4</sub> and Ne has been carried out (see section 4) with care to characterise the different transport channels up to the separatrix: electron and ion temperature, electron density, impurity density and toroidal rotation. C<sub>2</sub>D<sub>4</sub> was injected instead of N for better measurements with the edge CXRS diagnostics. In addition to the high- $\beta_N$  plasmas, further investigations of the effect of impurity were done with the earlier low- $\beta_N$  plasmas with the injection of CD<sub>4</sub> for improved measurements of the different pedestal channels during the recovery of the pedestal pressure (section 5). Prior to this work, an assessment of the MHD stability for the plasmas conditions is done (section 3).

## 3. ASSESSMENT OF PEDESTAL STABILITY WITH DIFFERENT MHD MODELS

The prediction of the plasma performance necessitates an understanding of the pedestal temperature and density height and in particular of how D-gas injection and impurities modify the pedestal temperature and density. The height is determined from the width and gradient in the steep gradient region. The temperature and density will evolve in the inter-ELM phase according to the transport mechanisms at play in the pedestal which is a mix of neoclassical transport and turbulence driven transport, such as Kinetic Ballooning Mode (KBM), Ion Temperature Gradient (ITG), Electron Temperature Gradient (ETG), Micro Tearing Modes (MTM) [6] [7] [8] and the pedestal particle source. The pedestal temperature height will be free to evolve with the constraint of the transport physics and ultimately determine the operating point (OP) at which the plasma becomes unstable to an ideal MHD mode called the peeling-ballooning mode (PB) and an ELM is triggered. One of the first items needed to be assessed is whether appropriate models for peeling ballooning stability can explain when the ELM is triggered.

The pedestal stability of the experimental plasmas is represented in the  $j$ - $\alpha$  stability diagram, where  $j$  is the current density, and  $\alpha$  the normalised pedestal pressure gradient. When assessing the edge stability, the pressure pedestals with the carbon wall are consistently found close the PB limit before an ELM crash. In this case, the experimental alpha  $\alpha_{max}$  is approaching  $\alpha_{crit}$  which represents the maximum normalised pressure gradient expected by the P-B model. The conventional procedure used in the ELM stability analysis in JET-C and JET-ILW plasmas assume that the ion temperature is equal to the electron temperature profile and that the toroidal rotation  $\Omega_{tor}$  is negligible. The conventional procedure and the ideal MHD model have explained well the ELM trigger condition in JET-C. Results on JET-ILW ELM stability presented up-to-now in the literature have been done with this conventional model, apart from [9] [10]. In the dataset considered here, it was assessed that if  $T_i$  and  $T_e$  profiles are assumed equal, this leads to an overestimate of the  $\alpha_{max}$  value by 20% with respect to using the  $T_i$  experimental profile. This result would tend to increase the discrepancy in the distance between the  $\alpha_{crit}$  and the experimental  $\alpha_{max}$ . This 20% increase in the value  $\alpha_{max}$  is not dependent on the position of  $\alpha_{max}$ , with  $\alpha_{max}$  position varying from 0.97 to 0.99 for this dataset.

MINERVA-DI [11] is an MHD stability code that includes the ion diamagnetic drift ( $\omega_{*i}$ ) effect in rotating plasmas and analyse the PBM stability with these non-ideal effect [11]. In the paper, the validation work already done on 12 JET discharges reported in [9] is extended to additional shots at lower collisionality ( $v_{e,95}^* < 1$ ). Similarly, to the latter paper, three MHD models are used to analyse the PBM stability: the ideal MHD model without rotation (IDEAL, but with  $T_e$  and  $T_i$  value), the diamagnetic MHD model without (DIAwoR) and with rotation (DIAwR). The range of  $n$  numbers of PB modes analysed numerically is between 1 and 100. In [9], it was shown that plasma rotation can destabilize the peeling-ballooning modes and contributes to make the stability boundary close to the OP on the stability diagram. The comparison of the different stability models is presented in Fig. 1 and Fig. 2, for low and high the  $v_{e,95}^*$  plasmas respectively. These figures show the  $v_{e,95}^*$  dependence of the distance between the stability boundary and the operation point,  $\Delta\alpha$ , which is defined as  $\Delta\alpha = (\alpha_{crit} - \alpha_{max,op}) / \alpha_{max,OP}$ . Here  $\alpha_{crit}$  is  $\alpha_{max}$  value at the stability boundary where  $\langle j_{ped,max} \rangle$  is equal that on the OP.

The error bars of  $\Delta\alpha$  are determined by estimating  $\alpha_{\max}$  on the boundary where  $\langle j_{\text{ped,max}} \rangle$  is changed by  $\pm 20\%$  from the OP. A value of  $|\Delta\alpha|$  within 0.2 is considered acceptable in this study. At low  $v_{e,95}^*$  ( $v_{e,95}^* \leq 1$ ), the three MHD models, ideal DIAwoR and DIAwR can be applicable for the ELM stability but the last two models provided the closest  $\alpha_{\text{crit}}$  to the OP, as shown in Fig. 1. At low  $v_{e,95}^*$ , the ideal MHD models tend to underestimate the normalised pressure gradient with respect to the experiment. The  $\omega_i^*$  effect taken into account in the other two MHD models provides a closer prediction of the ELM trigger to the OP. The  $\Delta\alpha$  distribution for the plasma considered is similar for the DIAwoR and DIAwR model, highlighting that the rotation at low  $v_{e,95}^*$  does not have a significant effect. On the other hand, for the high  $v_{e,95}^*$  ( $>1$ ) plasmas considered here, both ideal and DIAwR models can be applicable for the ELM stability in JET-ILW. Unlike in the low  $v_{e,95}^*$  case, the rotation is clearly influencing the MHD stability as the DIAwR model is closer than the DIAwoR model to the trigger conditions. The IDEAL MHD model do have a major drawback both at low and high  $v_{e,95}^*$ . The most unstable toroidal mode is identified as  $n=100$  (see Fig. 1 and Fig. 2), the maximum mode number considered in the analysis. Such short wavelength modes are usually not regarded as the trigger of the type-I ELM and in fact the  $\omega_i^*$  effect stabilises high- $n$  ballooning modes. On the contrary, the DIAwR and DIAwoR MHD model have the most unstable toroidal mode number below 80.

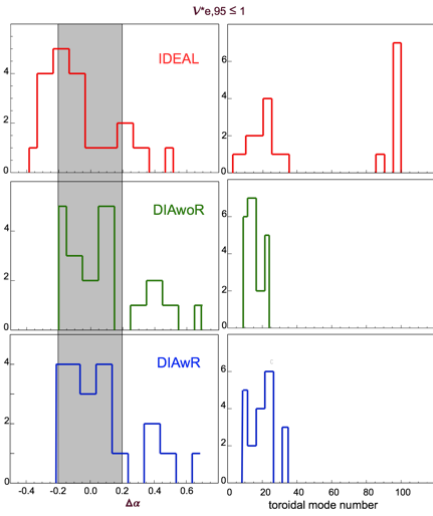


Fig. 1: Histogram of  $\Delta\alpha$  value (left) and most unstable mode number (right) for each MHD model with plasma with  $v_{e,95}^* \leq 1$ . Shaded region indicated  $|\Delta\alpha| \leq 0.2$ .

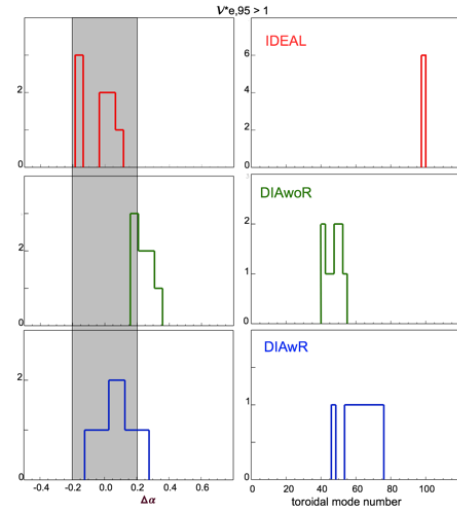


Fig. 2: Histogram of  $\Delta\alpha$  value (left) and most unstable mode number (right) for each MHD model with plasma with  $v_{e,95}^* > 1$ . Shaded region indicated  $|\Delta\alpha| \leq 0.2$ .

In summary, the DIAwR MHD model is best able to understand the ELM trigger conditions and determine the most unstable mode for most of the high and low  $v_{e,95}^*$  plasmas in this dataset. Nevertheless, the distance  $\Delta\alpha$ , in particular, some low  $v_{e,95}^*$  plasmas remain outside the acceptable domain with the DIAwR model. It is possible that the resistivity, not included in the present model, destabilizes high- $n$  PB mode [10], but no dependence of the  $\Delta\alpha$  value with  $v_{e,95}^*$  is observed. On the other hand, the value of  $\Delta\alpha$  increases as the ELM frequency increases. Apart from one plasma, the value of  $|\Delta\alpha|$  determined with DIAwR was above 0.2 when the ELM frequency was above 100Hz. Note that the time resolution of the edge CXRS system of 7.2ms, which limits the probing to plasma below the ELM frequency of 100Hz. For the dataset considered here, with excellent electron, ion temperature and toroidal rotation data, the DIAwR MHD model can determine  $\alpha_{\text{crit}}$  within 20% of  $\alpha_{\max}$ , provided the ELM frequency is low enough with respect to the integration time of the edge CXRS diagnostic. Note that the poloidal and toroidal rotation of the main ions used in the stability calculations are deduced from neoclassical theory [10].

#### 4. ANALYSIS OF HIGH-BN PLASMAS WITH SCAN IN D AND IMPURITY

##### 4.1. Difference in confinement and pedestal height for tile 5 and tile 6 configurations

In the high- $\beta_N$  plasma (see section 2), two datasets were obtained with a slightly modified magnetic configuration due to operational constraints. A first dataset was obtained with a scan in D-gas and  $\text{C}_2\text{D}_4$ -gas with the outer divertor leg on tile 5, and, in another dataset, a scan in Ne-gas and D-counterpart were done in tile 6 configuration.

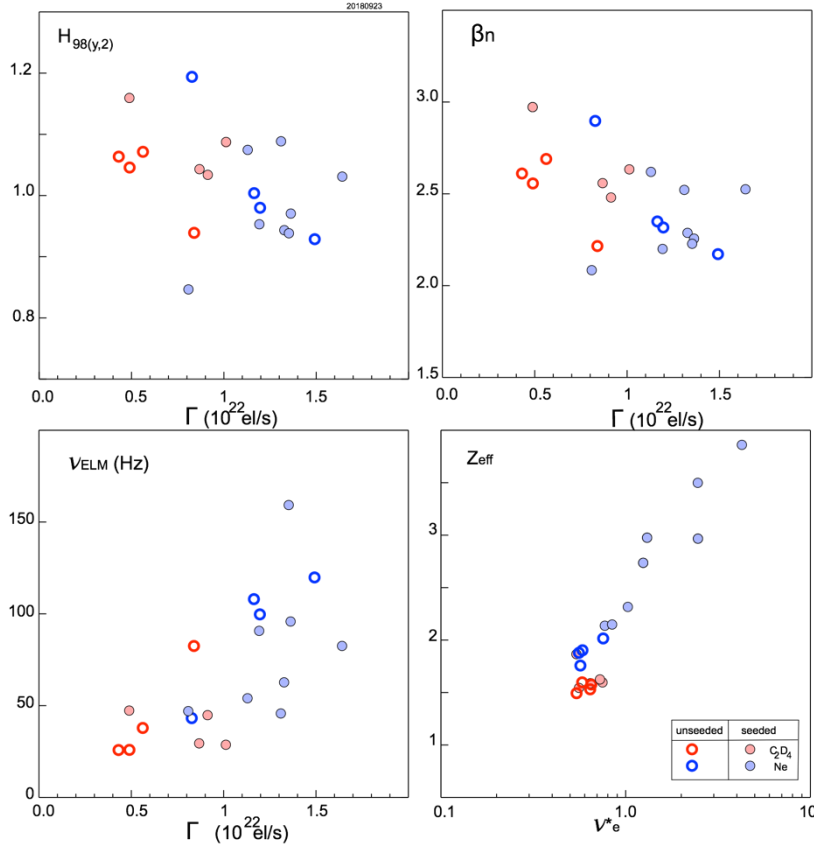


Fig. 3: (from top left to bottom right)  $H_{98(y,2)}$ , normalised pressure, ELM frequency versus total injected electron per second, and  $Z_{eff}$  versus pedestal collisionality for tile 5 dataset (red) and tile 6 dataset (blue), for unseeded (open symbols) and seeded (filled symbol for  $C_2D_4$  (red), Ne (blue)).

points of the magnetic configuration close to the divertor pump duct entrance (tile 6 configuration) leading to a reduction of the divertor neutral pressure, are required to recover the fusion performance with an confinement time enhancement factor close to unity [14]. This scan gives us the opportunity to understand better the change of confinement. As the D-gas rate is increased, the confinement is not maintained and similar value of  $H_{98}=0.9$ ,  $\beta_N=2.1$  is obtained, at a D-gas rate of  $0.8$  and  $1.5 \times 10^{22}$  el/s for tile 5 and 6 respectively. In the tile 6 configuration, the D-gas rate is higher than for tile 5 due to the outer strike point being closer to the pumping duct, and the D-gas being directly pumped. One striking observation is that the ELM frequency for the tile 6 configuration is higher than for tile 5 for similar value of  $H_{98}$  except for the higher confinement plasma on tile 6 at lowest D-gas rate, see Fig. 3. The  $Z_{eff}$  value is mostly dominated by medium-Z impurities such as Ni or Cu, and it is higher on tile 6 than tile 5.

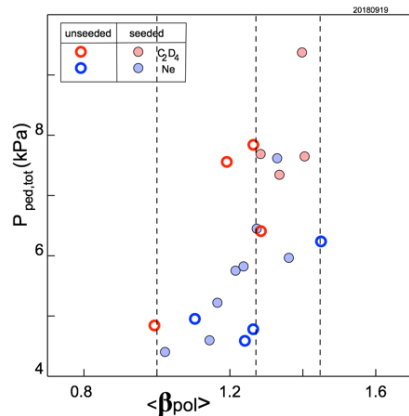


Fig. 4: total pedestal pressure versus volume averaged normalised poloidal pressure

A comparison of the total pedestal pressure between these two configurations is made versus the normalised volume averaged poloidal pressure  $\langle \beta_{pol} \rangle$ , as the core pressure increases the Shafranov shift which in turns has a stabilizing effect on the pedestal limited by the PB-modes [12] [13]. At an equivalent  $\langle \beta_{pol} \rangle$  value of  $\sim 1.25$ , the pedestal pressure is lower by a factor 1.7 with the tile 6 configuration compared to the tile 5 configuration, see Fig. 4. At the total pedestal pressure of  $\sim 6$  kPa, the pedestal of the two configurations can be similar, but the normalised poloidal pressure  $\langle \beta_{pol} \rangle$  is above 1.4 for the tile 6 and at 1.25 for the tile 5 configuration, respectively. This higher core contribution to the total pressure can be due to either higher peaking of the temperature and density or a higher value of the pedestal temperature and/or density.

The only difference in the magnetic configuration is that the outer leg on tile 6 is at a closer proximity to the pumping duct entrance. A study of the effect of D-gas alone is necessary prior to a comparison of the impact of a seeded impurity on the pedestal and confinement of these plasmas. [12] [13]. The discharges considered in these two datasets were carried at the same input power of 16.5-17.5 MW with a power flowing through the separatrix of 13 MW (unseeded) and provide a fair comparison of these two configurations with similar engineering parameters. The energy confinement at lower D-gas rate with tile 6 configuration is indeed above the values of the tile 5 configuration with  $H_{98}=1.2$ ,  $\beta_N=2.8$  with D-gas rate of  $0.8 \times 10^{19}$  el/s (see Fig. 3), exactly in line with observation made for JET-DT scenarios. It was empirically found, for the DT baseline scenarios developed in JET-ILW, that efficient pumping conditions with the strike-

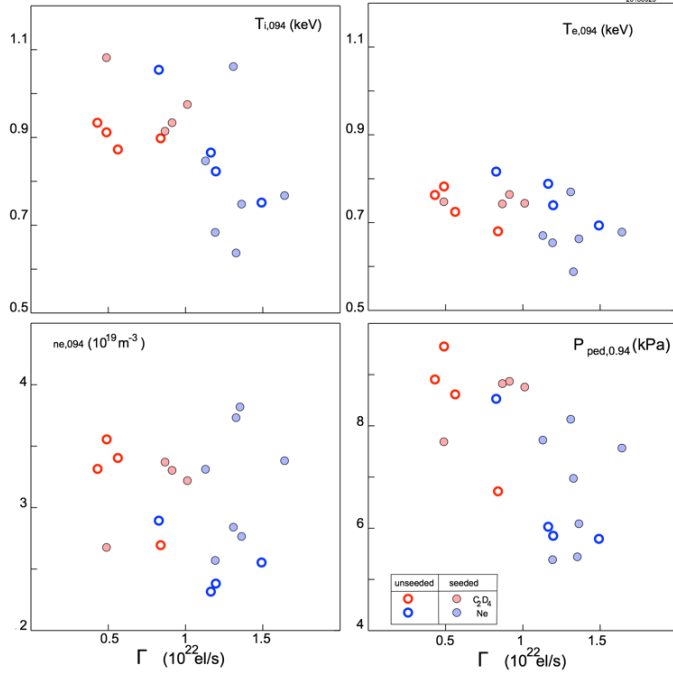


Fig. 5: (From top left to bottom right) Value of the pedestal ion temperature, electron temperature, total pedestal pressure and electron density versus total el/s injected rate.

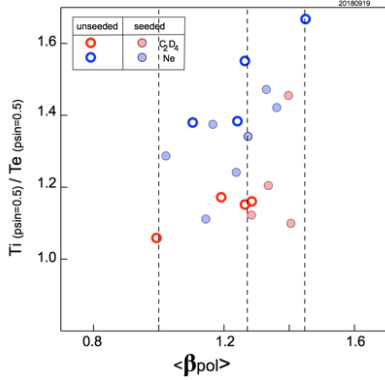


Fig. 6: ratio of the ion to electron temperature at mid-radius versus volume averaged normalized poloidal pressure.

#### 4.2. Impact of $C_2D_4$ and Ne on the pedestal height and confinement in high- $\beta_N$ plasmas

$C_2D_4$  was injected in the plasma with the tile 5 configuration such that the total number of electron puffed per second was constant to the low and high el/s injected of their unseeded counterpart plasmas, see Fig. 5. The injection of  $C_2D_4$  increases the energy confinement time and normalised pressure both at low and high el/s rate in comparison to the unseeded plasmas, see Fig. 4. The ELM frequency is increased at low el/s rate from 20 to 40Hz and decreased at high el/s rate from 80 to the 20Hz. The  $Z_{eff}$  value is not affected by the quantity of  $C_2D_4$  injected at high el/s rate and the electron collisionality remains unaffected. As D-gas rate is increased in the unseeded plasmas with tile 5 configuration, the pedestal  $T_e$  decreases steadily but the pedestal  $T_i$  remains constant. The pedestal electron density drops at high el/s rate. In contrast,

the injection of  $C_2D_4$  at high el/s rate leads to an increase of the electron density and electron temperature back to the level of the unseeded low el/s D-gas rate with in addition an increased pedestal ion temperature, see Fig. 5. The C concentration is then below 0.33%. The unseeded plasma with the highest D-gas injection had the lowest value of  $\langle\beta_{pol}\rangle \sim 1$ , but the injection of  $C_2D_4$  keeping the total rate of injected el/s constant led to an increase of  $\langle\beta_{pol}\rangle$  to 1.4 and an increase of the total pedestal pressure from 4.7kPa to 7.4kPa, see Fig. 5. As a result, the ratio of  $T_i/T_e$  at mid-radius is re-established to the level of the low D-gas el/s rate. The OP in the  $j$ - $\alpha$  diagram shows that the OP with  $C_2D_4$  seeding at high el/s recovers the domain of the OP of the unseeded plasmas at low el/s, see Fig. 7. At low el/s injection rate, the  $C_2D_4$  leads to an increase of the pedestal ion temperature by a factor 1.22 ( $C_C=0.5\%$ ) leading a  $T_i$  at mid-radius of 4keV (similar value to the unseeded tile 6 plasmas at  $\langle\beta_{pol}\rangle \sim 1.4$ ), a reduction of the pedestal electron density and no improvement in the electron density. The normalised pressure  $\beta_N$  is then increased from 2.6 to 3 and  $H_{98(y,2)}$  from 1.05 to 1.15. More data points may be needed at low el/s injection rate for a clear conclusion.

The injection of Ne in the high- $\beta_N$  plasmas can be the overall energy confinement and pedestal with respect to the unseeded discharges at the same el/s injection rate. It was observed in three discharges (#90171, #90174, #90175) at  $1-1.7 \times 10^{22}$  el/s,  $c_{Ne} \sim 0.6-1.1\%$ . The normalised pressure is able at best to increase from 2.1 to 2.5, and

The key overall differences between the pedestal of the two configurations are the lower electron pedestal density plasmas, and a higher pedestal ion temperature at the lowest D-gas rate, both for tile 6 plasmas see Fig. 5. At the value of  $\langle\beta_{pol}\rangle \sim 1.25$ , an increased peaking of the profile is therefore necessary to explain the increased core pressure. It is the difference in the ion temperature peaking which results in a significant contribution from the ion temperature to the total pressure in the tile 6 configuration as seen from the ratio of  $T_i/T_e$  in Fig. 6. At  $\langle\beta_{pol}\rangle = 1.4$ , the high value of  $T_i/T_e$  resulting more from an increased pedestal  $T_i$  than increased  $T_i$  peaking. This physics is relevant to the DT-scenarios as the decoupling of the electron and ion temperature leading to an increase of the total pressure was observed recently to be the cause for the improved confinement in JET-DT discharges [15].

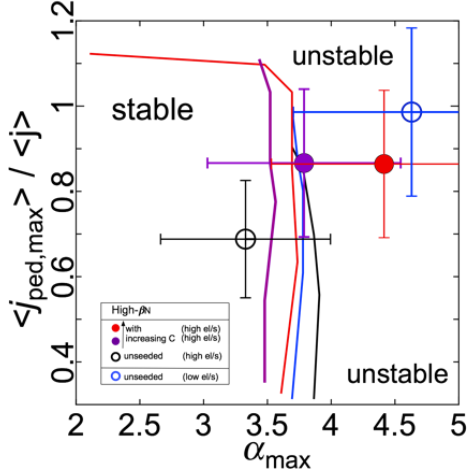


Fig. 7:  $j$ - $\alpha$  diagram calculated with MINERVA-DI at low (#92168) and high el/s (#92167) with increasing C (#92174, #92176) at high el/s

normalised energy confinement from 1.0 to 1.09, with an ELM frequency which is almost in all cases decreased and a value of  $Z_{eff}$  at best of 2.1 or higher. The main reason for the increase in energy confinement is due to an increase in electron pedestal density (see Fig. 5). Ne can counter balance the effect of high el/s D rate on the pedestal electron density but not on the electron and ion temperature as does the  $C_2D_4$ . Only one discharge (#90171) shows sign of a high ion temperature and electron temperature with respect to the unseeded plasmas at similar el/s injection rate and it is the lowest Ne concentration ( $c_{Ne} \sim 0.6\%$ ) and lowest pedestal radiation losses due to Ne. Similar results were obtained in AUG with Ne and N-seeding [16]. On JET-ILW, seeding of Ne results in opposite behaviour on the pedestal density depending on  $v_e^*$  and  $\beta_N$ , but in none of the cases does Ne seeding lead to an increase of temperature, unlike C.

## 5. ANALYSIS OF LOW- $\beta_N$ PLASMAS WITH $CD_4$

The pedestal recovery was also investigated in low- $\beta_N$  plasmas with  $CD_4$  injection in the original scenarios where the N-seeding led to the recovery of the pedestal pressure [4]. The operational domain probed here was at a higher D-gas injection than done previously,  $3.7 \times 10^{22}$  el/s, and it was observed that the recovery of the pedestal pressure with N-seeding or  $CD_4$ -seeding was not always taking place. With the total input power kept constant, the addition of  $CD_4$  ( $1.73 \times 10^{22}$  el/s) on top of a D-gas rate of  $3.7 \times 10^{22}$  el/s (#89452), lead to no significant increase of stored energy ( $H_{98} \sim 0.7$ ). The ELM frequency has increased from 56Hz (unseeded) to 96Hz. On the other hand, if the D-gas is reduced to  $1.7 \times 10^{22}$  el/s with  $CD_4$  maintained at  $1.26 \times 10^{22}$  el/s (#89453), the stored energy is steadily increasing in time and reach an energy confinement time of 0.28 (an increase of 27%),  $\beta_N$  of 1.45,  $H_{98}$  of 0.79. The ELM frequency is reduced to 28Hz, characteristic of the improved confinement in N-seeding plasmas [4]. A threshold is therefore observed at high D-gas injection of high el/s injection where the injection of C cannot lead

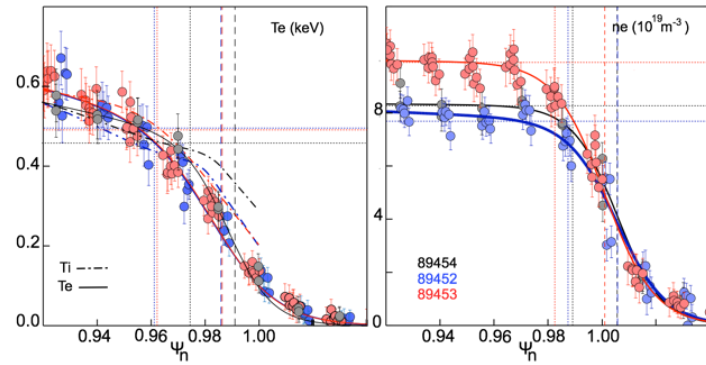


Fig. 8: Pedestal electron and ion temperature profile (left), and electron density (right) versus  $\psi_n$ , for #89454 (back), #89452 (blue) and #89453 (red).

to an increase of pedestal pressure (also observed with N). The power crossing the separatrix ( $P_{sep} = P_{in} - P_{rad} - dW/dt$ ) in these three discharges remains similar,  $P_{sep} = 9.5$  MW (89454), 10 MW (89452), 8.5 MW (89453). The carbon concentration for both seeded pulses (#89453 and #89452) is in the range 0.7-0.8%. The electron temperature profiles between (#89453 and #89452) are similar as are the ion temperature profiles. The pulse #89453 with improved energy confinement has a higher density and a higher value  $a/L_n$  in the pedestal, see Fig. 9. This results in a value of the normalised pressure gradient for #89453 to be similar to the unseeded plasma (#89454), of about

$\alpha_{max} \sim 3.5$  but higher than the seeded plasma #89452 ( $\alpha_{max} \sim 2.6$ ). The increased pedestal width in #89453 than leads to an increased pedestal pressure.

## 6. TRANSPORT AND GYROKINETIC CALCULATIONS

A radially global neoclassical modelling of JET plasmas was performed with PERFECT [17], using experimental magnetic geometry. It allowed the study of neoclassical transport and flows in JET pedestals. The neoclassical ion heat flux is found to be approximately an order of magnitude smaller than the input power [18]. The small neoclassical transport is consistent with the shallow ion temperature profiles (inferred from  $C^{6+}$ , assuming  $T_i = T_C$ ). Unless the electron energy flux is an order of magnitude larger than the ion heat flux, it suggests that the ion heat transport is not neoclassical in the JET pedestal, but it is carried by a significant remnant ion scale turbulence,

which is in line with the results of [8]. The size of the momentum transport is more strongly correlated to density steepness than impurity content but is likely insignificant.

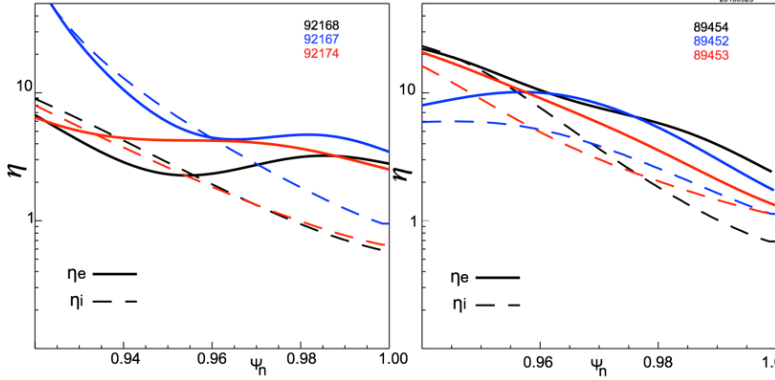


Fig. 9:  $\eta_e$  (filled) and  $\eta_i$  (dashed) for the high- $\beta_N$  (left) and low- $\beta_N$  plasmas (right)

#89453 has a lower  $\eta_e$  value than #89454 or #89452 within the pedestal as could be expected from an improved pedestal pressure. Similarly, pulses #92174 ( $C_2D_4$  at high el/s) and #92168 unseeded at low el/s) have a reduced value of  $\eta_e$  with respect to #92167 (unseeded at low el/s), with a reduced pedestal pressure. An estimate of the impact of the particle source over the heat flux has been carried out. Interpretative EDGE2D modelling of the high- $\beta_N$  plasmas have been carried out and reproduced well the pedestal and SOL profiles. From these runs, the particle source  $S$  is estimated small in comparison with the heat flux from the core ( $S \cdot T / Q_{tot} < 0.05$ ), therefore processes with little density transport, relative to the energy transport (such as MTM and ETG) are the most likely heat transport mechanisms [19]. A similar estimate was done for the low- $\beta_N$  plasmas, from similar EDGE2D runs as the interpretative EDGE2D modelling are not yet available. Using the measured  $\eta$ , it can be estimated that  $D_{eff} / (\chi_{eff}) \sim 0.1-0.18$  or less. This is inconsistent with MHD-like modes being a major player in the energy loss [7] [19] and again points to mechanisms like ETG and MTM.

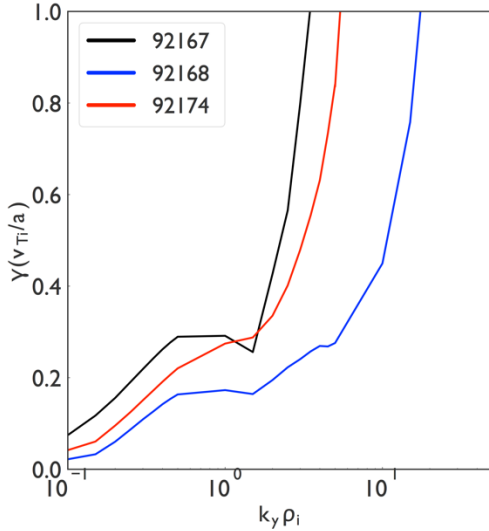


Fig. 10: Growth rate calculated from linear GS2 for high- $\beta_N$  plasmas respectively low (#92168) and high D-gas (#92167), high el/s rate with  $C_2D_4$  (#92174) at radius for  $a/Ln \sim 2$

The gyrokinetic analysis of these low and high- $\beta_N$  plasmas is on-going. The following has been found so far. Linear gyrokinetic calculations performed with GS2 on the high- $\beta_N$  plasmas, revealed the Electron Temperature Gradient (ETG) to be the main linear instability drives even at ion scales. Unexpectedly, the ion scale instabilities are not Trapped Electron Modes (TEM), but toroidal ETG modes aided by a non-adiabatic ion response [20]. At the electron scale, instabilities are predominantly slab ETG modes. Quasilinear estimates indicate that the electron heat flux is 1.5 to 3 times larger than the ion heat flux. Flow shear appears ineffective at suppressing linear instabilities across a wide range of  $k_y$  modes. Unseeded plasmas at low el/s injection rate and with  $C_2D_4$  at high el/s injection rate (#92168, #92174) result in a lower growth rate than the unseeded plasmas at high el/s rate at lower  $k_y$ . Non-linear calculations are on-going to assess the associated transport.

The low- $\beta_N$  plasmas were also investigated with GENE. The linear gyrokinetic calculation suggests that ETG dominates the heat transport in all three cases, as would be expected for a high  $\eta_e$ . Nonlinear ETG simulations indicate that heat fluxes are at experimentally relevant levels. ETG transport is lower for 89453, as expected from a steeper density gradient and lower  $\eta_e$ . ETG transport is consistent with the high heat diffusivity, low particle diffusivity, and early saturation of the electron temperature in the ELM cycle. However, it remains to be explained why the electron density increases in #89453. Potential explanations include: an increase in the pedestal particle source; changes in ETG particle transport due to kinetic ion behaviour at scales approaching the ion scales; and ion-scale transport mechanisms (ITG and/or TEM) that may operate at low fluctuation levels affecting predominantly the particle channel.

## 7. CONCLUSION

Robust predictions for the pedestal temperature and density in ITER requires an understanding of the role that D-gas and seeded impurity, such as N and Ne, have on pedestal temperature and density in JET-ILW. Both low- $\beta_N$  and high- $\beta_N$  plasmas were investigated. It was observed that CD<sub>4</sub> and C<sub>2</sub>D<sub>4</sub> can increase the pedestal density at high el/s injection. In high- $\beta_N$  plasmas, C<sub>2</sub>D<sub>4</sub> can counteract the degradation of electron temperature and density at high rate of D injection and raise the pedestal ion temperature. On JET-ILW, seeding Ne can result in a decreased or increased pedestal density depending on pedestal collisionality and  $\beta_N$ . Ne seeding decreased the electron pedestal density and temperature in low- $\beta_N$  plasmas but was able to increase the electron density in the high- $\beta_N$  plasmas. Nevertheless, in all cases seeding Ne does not lead to an increase of ion or electron temperature, unlike C (or N in earlier low- $\beta_N$  plasmas), highly likely due to increased pedestal radiation losses with Ne. Even in unseeded plasmas, a reduction of electron density due to increased pumping was shown to give access to a higher confinement due an increase of the ion temperature peaking and even a higher ion temperature at the pedestal for low el/s. With a linear MHD code taking into account the effect of rotation and ion diamagnetic effect, it was possible to determine the ELM trigger conditions  $\alpha_{crit}$  within 20% of the value a maximum normalised gradient  $\alpha_{max}$ . The key issue then remains to understand the change in the pedestal temperature and density response. It is not clear if changes to the pre-ELM behaviour of the density and temperature with D-gas or seeded impurity is due to a change of instabilities, a reduction of transport due the dominant instabilities, a modification of the ionisation sources, an increased radiation loss, a combination of these effects. This identification work has just started. The ion heat transport is not neoclassical in the JET pedestal. In the low and high- $\beta_N$  plasmas investigated in this paper the dominant instabilities leading to the energy losses is Electron Temperature Gradient, which can unexpectedly lead to losses at ion scale. It is clearly a complex problem linking core, pedestal and SOL physics which will require dedicated and continuous effort to disentangle the different possible effects in the coming years.

Acknowledgment: This work has been carried out within the framework of the EUROfusion Consortium and has received funding from the EURATOM research program 2014-2018 under grant agreement No. 633053. The views and opinions expressed herein do not necessarily reflect those of the European Commission.

## REFERENCES

- [1] M. Beurskens and et al, *Nucl. Fusion*, vol. 54, p. 043001, 2014.
- [2] C. Maggi and et al, *Nucl. Fusion*, vol. 55, p. 113031, 2015.
- [3] I. Nunes and et al, *Plasma Phys. Control. Fusion*, vol. 58, p. 014034, 2016.
- [4] C. Giroud, *Nucl. Fusion*, vol. 53, p. 113025, 2013.
- [5] C. Giroud, in *IAEA*, St Petersburg, 2014.
- [6] P. Snyder, *Nucl. Fusion*, vol. 51, p. 103016, 2011.
- [7] M. Kotschenreuther, D. Hatch, S. Mahajan and e. al, *Nucl. Fusion*, vol. 57, p. 064001, 2017.
- [8] D. Hatch and et al, *Nucl. Fusion*, p. 036020, 2017.
- [9] N. Aiba, *Plasma Phys. Control. Fusion*, vol. 60, p. 014032, 2018.
- [10] N. Aiba, *Nucl. Fusion*, vol. 57, p. 126001.
- [11] N. Aiba, *Plasma Phys. Control. Fusion*, vol. 58, p. 045020, 2016.
- [12] P. Snyder, *Nucl. Fusion*, vol. 47, p. 961, 2007.
- [13] S. Saarelma, *Physics of Plasmas*, vol. 22, p. 056115, 2015.
- [14] L. Garzotti, in *IAEA*, Ghandinagar, 2018.
- [15] H.-T. Kim, *Nucl. Fusion*, p. 036030, 2018.
- [16] M. Dunne, *Plasma Phys. Control. Fusion*, vol. 59, p. 025010, 2017.
- [17] M. Landreman, *Plasma Phys. Control. Fusion*, vol. 56, p. 045005, 2014.
- [18] I. Pusztai, S. Buller and et al, "[https://users.euro-fusion.org/tfwhttps://users.euro-fusion.org/tfwiki/images/9/93/PerfectT17-9\\_V02\\_2018-09-26.pdf](https://users.euro-fusion.org/tfwhttps://users.euro-fusion.org/tfwiki/images/9/93/PerfectT17-9_V02_2018-09-26.pdf)," 2017. [Online].
- [19] M. Kotschenreuther and et al, in *IAEA*, Ahmenabad, India, 2018.
- [20] J. Parisi and F. Parra, in *preparation*, 2018.